PCCP

Crystal-size effect on the kinetics of CO$_2$ adsorption in metal organic frameworks studied by NMR

SCHOLARONE™
Manuscripts

Crystal-size effect on the kinetics of CO_2 adsorption in metal organic frameworks studied by NMR[†]

Weiming Jiang[a] and Kazuyuki Takeda[*a]

We study the dynamics and the exchange of carbon dioxide (CO_2) adsorbed in a metal organic framework (MOF) by ^{13}C NMR for various sizes of the host crystal ranging from micrometers to millimeters. We found that the guest CO_2 molecules adsorbed in $[Zn_2(1,4-NDC)_2(dabco)]_n$ MOF undergo exchange at a rate that depends on the size of the host crystal, revealing that the smaller the host crystals are, the faster the exchange becomes. Such a trend can be explained by the size-dependent surface-to-volume ratio.

1 Introduction

Metal-organic frameworks (MOFs) are a class of porous materials assembled with metal clusters and organic linkers. The diverse applications of the MOFs, such as gas storage/separation[1,2], catalysis[3], drug delivery[4], sensing[5], and so on, rely on the host-guest interactions at the active surface sites. Thus, the functions of the MOFs can be tuned by controling the particle size and thereby the surface area, as well as by straightforward chemical modification. Indeed, many reports addressed the consequences of adjusting the particle size that manifest through macroscopic observations of, e.g., the catalytic activity[6], adsorption efficiency[7–9], optical properties[10], shape memory[11,12], and so on. However, little has been investigated about the particle-size effect from a microscopic, molecular perspective.

Nuclear magnetic resonance (NMR) is a powerful tool for probing local structure and dynamics, and has extensively been used in studies of the MOFs regarding the host-guest interactions and the dynamics of the guest molecules. For instance, through ^{13}C NMR studies, Kong et al. reported that the carbon dioxide (CO_2) molecules adsorbed in MOF-74 undergo rotational motion[13]. An alternative model involving translational, hopping motion for the CO_2 molecules in the same MOF was proposed by Lin et al.[14] The rotational/translational dynamics of CO_2 adsorbed in a different MOF, namely, DMOF-1, was studied by Peksa et al., who also reported anisotropy of diffusion[15,16]. Forse et al. reported diffusion anisotropy of CO_2 in $Zn_2(dobpdc)$[17]. Even though such microscopic, molecular-scale studies using NMR have been successful, most have so far overlooked the the particle-size effect.

Here, we bridge such a gap found in the current NMR researches on gas adsorption in the MOFs, both investigating dynamics of the guest molecules and addressing the size effect. In this work, we report ^{13}C NMR studies on the crystal-size dependence of the kinetics of the CO_2 molecules adsorbed in $[Zn_2(1,4-NDC)_2(dabco)]_n$ MOF (NDMOF, Fig. 1) for crystal sizes ranging from micrometers to millimeters. As shown below, ^{13}C NMR spectra of CO_2 adsorbed in a millimeter-sized single-crystal reflect the motion of the CO_2 molecules inside the crystal of ND-

MOF. As downsizing the NDMOF crystals, the profile of the ^{13}C resonance line changes significantly. To account for the shapes of the observed resonance lines, we propose a model for gas exchange, extracting the crystal-size-dependent kinetic parameters. The present work also supports the inter-particle exchange for the origin of the particle-size-dependent chemical shift anisotropy found in the MOFs that show size-dependent flexibility[8,18], as suggested by Melix and Heine, who excluded the possibility of the size-dependent flexibility for the cause of the change in the chemical shift anisotropy with the particle size[19].
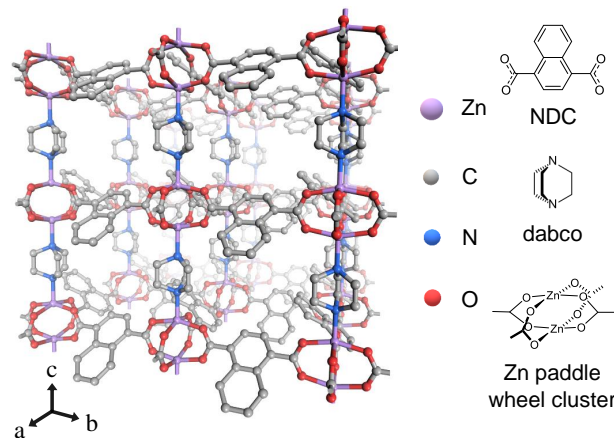
Fig. 1 Structure of $[Zn_2(1,4-NDC)_2(dabco)]_n$ MOF (NDMOF). Hydrogen atoms are not shown for clarity.

2 Experimental

We synthesized NDMOF according to a procedure described in Supplementary Information[†] and prepared several CO_2-loaded NDMOF crystals with various sizes. The samples include a single crystal (referred to as sc@CO_2) with a size of 1–2 mm, gently crushed crystals (cc@CO_2) composed of microcrystals with sizes of 100–200 μm, coarse powder (pd@CO_2) and fine powder (spd@CO_2) with crystallites of 10–20 μm and 1–2 μm in size. The crystal structure was characterized by power X-ray diffraction (Figs. S1 and S2), and the particle size was estimated from SEM images (Figs. S3 and S4). The individual sample was put in a glass tube and evacuated before being flame-sealed together with ^{13}C-labeled CO_2 with pressure of 90 kPa.

[a] Division of Chemistry, Graduate School of Science, Kyoto University, 606-8502 Kyoto, Japan.

[*] E-mail: takezo@kuchem.kyoto-u.ac.jp

3 Results and Discussion

3.1 Single crystal ^{13}C NMR

Figure 2 shows ^{13}C spectra of sc@CO_2, i.e., ^{13}C-labeled CO_2 loaded in a single crystal of NDMOF, measured at 303 K in a static magnetic field B_0 of 7.05 T with different orientations of the crystal with respect to B_0. This magnetic field corresponds to the ^{13}C Larmor frequency of 75.3 MHz.

When the c-axis of the crystal was aligned along B_0, the ^{13}C chemical shift was 107 ppm (Fig. 2a). When the a- or the b-axis was parallel to B_0, the chemical shift was 155 ppm (Fig. 2c). We found that the chemical shifts for any other directions of the crystal were in-between these values (Fig. 2b). The results are similar to those reported by Forse et al. for Zn_2(dobpdc), a different type of MOF[17].
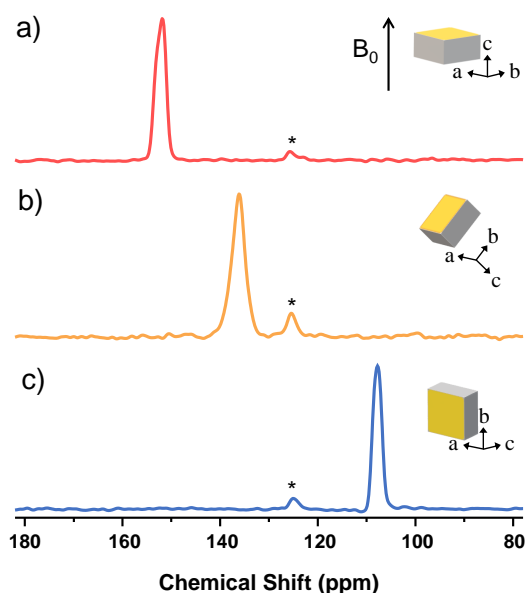
Fig. 2 ^{13}C spectra of sc@CO_2 obtained with (a) the c-axis parallel to the external field B_0, (b) arbitrary crystal orientation, and (c) the b-axis aligned along B_0. The peaks indicated by the asterisks are assigned to be free CO_2 gas.

For pure CO_2 in the rigid solid state below its sublimation temperature, the ^{13}C chemical shift tensor is axially symmetric with the principal values $(\delta_{11}, \delta_{22}, \delta_{33})$ of $(230, 230, -85)$ ppm, so that the isotropic shift δ_{iso}, given by

$$\delta_{iso} = \frac{1}{3}(\delta_{11} + \delta_{22} + \delta_{33}), \qquad (1)$$

is 125 ppm in the present case. The limited range (107 to 155 ppm) of the ^{13}C chemical shift in sc@CO_2 compared to that (-85 to 230 ppm) in the solid CO_2 and the observed sharp ^{13}C resonance line indicate that the CO_2 molecules undergo fast reorientation, causing partial averaging of the chemical shift anisotropy. The CO_2 molecules adsorbed in NDMOF also move from one pore to another. Even though full description of the dynamics of the guest molecules should thus include the translational motion of the center of gravity as well as the molecular reorientation, the

former does not affect the NMR lineshape. It follows that, at least in lineshape analysis, we can use a model in which the guest molecules behave as if they undergo reorientation at a fixed place, albeit they *do* translate as well.

The observed chemical shift can be explained by a model in which the individual CO_2 molecule adsorbed inside the pore of NDMOF gyrates rapidly around the c-axis of the crystal, such that the molecular axis draws a pair of cones with the carbon atom being the apex. In this *gyration model*, the chemical shift anisotropy scales with $(3\cos^2\theta - 1)/2$, where θ is the angle between the molecular axis of CO_2 and the c-axis of NDMOF. Out of the two possibilities for θ, namely, 49° and 61°, we take the latter, i.e., $\theta = 61°$, because it leads to the same isotropic shift as that of rigid CO_2. We henceforth call the region in which the gyration model is valid as the *core sites*. We also found that the resonance line of the sc@CO_2 broadens considerably at temperatures below -40 °C (Fig. S5). Such a low-temperature regime in which the gyration model no longer holds is beyond the scope of this work.
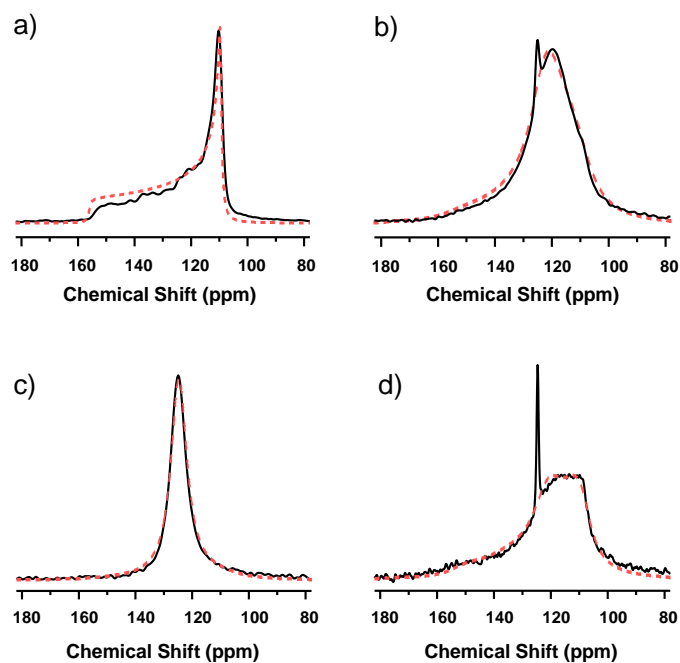
Fig. 3 Solid lines show experimental ^{13}C spectra of (a) cc@CO_2, (b) pd@CO_2 and (c) spd@CO_2 obtained in 7.05 T. (d) shows a ^{13}C spectrum of pd@CO_2 measured in 14.09 T. All data were taken at room temperature. Broken lines represent calculated spectra. In (a), the spectrum was calculated using the gyration model with an apex angle of 61°, while the other calculated spectra were obtained according to the isolated exchange model described in 3.3 with (b) $\omega_0/2\pi = 75.3$ MHz, $k_B = 200$ Hz, $p_B = 0.628$, $R_A = R_B = 220$ Hz, (c) $\omega_0/2\pi = 75.3$ MHz, $k_B = 200$ Hz, $p_B = 0.115$, and (d) $\omega_0/2\pi = 150.9$ MHz, $k_B = 200$ Hz, $p_B = 0.790$, $R_A = R_B = 320$ Hz

3.2 Polycrystalline ^{13}C NMR and crystal-size dependence

Figure 3a shows a ^{13}C spectrum of cc@CO_2, i.e., ^{13}C-labeled CO_2 loaded in the sample of microcrystals of NDMOF with the size of the order of 100 μm. We found that the experimental spectrum was well reproduced by an axially symmetric powder pattern $I(\omega)$

represented as[20]

$$I(\omega) = \frac{1}{2}\left[\omega_0(\delta'_{33}-\delta'_{11})(\omega-\omega_0\delta'_{11})\right]^{-\frac{1}{2}}, \qquad (2)$$

where $\omega_0 = -\gamma B_0$ is the Larmor frequency with γ being the gyromagnetic ratio. $\delta'_{11} = \delta'_{22}$ and δ'_{33} are the principal values of the chemical shift tensor under rapid gyration, expressed using those δ_{jj} $(j=1,2,3)$ for the rigid condition as

$$\delta'_{jj} = \delta_{jj} \cdot \frac{1}{2}(3\cos^2\theta - 1) \qquad (3)$$

with $\theta = 61°$. The broken line in Fig. 3a is a plot of convolution of $I(\omega)$ with a Lorentzian function with a width of 75 Hz.

Conversely, we observed striking differences in the line shape of the ^{13}C spectra of CO_2 loaded in the finer NDMOF powder samples, as demonstrated in Fig. 3b for pd@CO_2 ($\sim$10 μm) and Fig. 3c for spd@CO_2 ($\sim$1 μm). For pd@CO_2, the range in which the resonance lines appeared (107 to 155 ppm) was similar. Since the structure is common for all samples, the gyration of the CO_2 molecules inside the pore surrounded by the lattices of NDMOF ought to remain unchanged. Thus, the observed change in the spectrum as downsizing the particle is ascribed to exchange of the CO_2 molecules from one site to another with a rate comparable to or larger than the width of the ^{13}C resonance line for the case of negligible exchange. For spd@CO_2, the pattern was narrower, and the position of the peak was close to the isotropic chemical shift of the free CO_2 gas. This trend implies that the smaller the size of the NDMOF crystallites are, the faster the exchange becomes. The presence of exchange also implies that the adsorbed guest CO_2 molecules are not bound to specific pore sites. They rather undergo diffusion across the pores. The smaller the particle is, the more guests locates in the surface, and therefore the more prominent the exchange becomes.

3.3 Site exchange

Considerable change in the lineshape for the different crystal sizes is ascribed to that the surface and the volume scale differently with the size of the crystallite. The powder samples are composed of an assembly of tightly-packed microcrystals. When the guest CO_2 molecules move from the core site of one crystallite to that of another, they go through the interface between them. The CO_2 molecules are free from steric hindrance and rotate isotropically at the interface space, in contrast to the core sites where the motion of CO_2 molecules are confined to cone gyration. Since the isotropically-rotating CO_2 molecules do not retain the memory of which crystallite they were desorbed from, the upcoming process of re-adsorption to the other crystallites with any orientations in the powder sample is equally probable. Such multi-site exchange is schematically depicted in Fig. 4a.

Conversely, looking from inside the individual, *single* crystallite, we see that the guest CO_2 molecules just go to and come from the place where the ^{13}C spins are subject to the isotropic chemical shielding. One cannot tell whether the CO_2 molecules coming from the isotropic sites into the core sites of the current crystallite originate from the other crystallites or, with coincidence, belonged to the same one. Then, when we extend the view to see
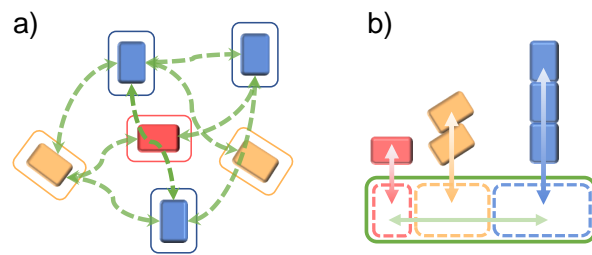
Fig. 4 Schematic diagram of (a) the multi-site exchange among crystallites through gaseous phase, (b) the isolated exchange model. Crystallites of different orientations are depicted with differently-colored boxes. The solid and open boxes represent the core site and the isotropic site, respectively. The pathways of exchange are indicated by the arrows.

the other crystallites and consider the evolution of the net macroscopic ^{13}C magnetization of CO_2 during signal acquisition, we see that the NMR spectrum under multi-site exchange among differently oriented crystallites via the free space (Fig. 4a) would be identical to that for an assembly of *separate, isolated* exchanges between the core site and the isotropic site (Fig. 4b). That is, as long as we focus on one-dimensional NMR, the multi-site exchange model may be reduced to a model of a set of isolated pairs of exchanging sites, one of which is the isotropic site, while the other is the randomly oriented core site.

To apply this isolated two-site exchange model, let us consider a given pair of sites, A and B, with exchange rates k_A and k_B:

$$(\mathbf{A})\text{NDMOF@}CO_2 \underset{k_B}{\overset{k_A}{\rightleftharpoons}} (\mathbf{B})\text{NDMOF@}CO_2. \qquad (4)$$
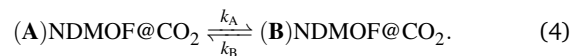
Let ω_A and ω_B be the resonance frequencies for site A and site B when exchange is negligibly slow, for which case a pair of separate peaks would appear with intensities given by $I(\omega_A)$ and $I(\omega_B)$. The effect of exchange is to result in the shape $J(\omega;\omega_A,\omega_B)$ of the resonance line given by[21,22]

$$J(\omega;\omega_A,\omega_B) = \text{Re}\left[\frac{k_A+k_B+p_A\alpha_B+p_B\alpha_A}{\alpha_A\alpha_B+k_A\alpha_B+k_B\alpha_A}\right], \qquad (5)$$

with

$$\alpha_A = R_A - i(\omega_A - \omega), \qquad (6)$$

$$\alpha_B = R_B - i(\omega_B - \omega). \qquad (7)$$

Here, p_A and $p_B = 1 - p_A$ are the populations, and R_A and R_B are the relaxation rates at sites A and B.

To calculate the lineshape $K(\omega)$ according to our model, we set site A to be the isotropic site ($\omega_A = \omega_0\delta_{iso}$), calculated the lineshape functions for various values of ω_B according to Eq. (5), and summed up the results with the weighting factor given by the experimental lineshape $I(\omega_B)$ of the cc@CO_2 sample. That is, the lineshape $K(\omega)$ is represented as

$$K(\omega) = \int d\omega_B I(\omega_B) J(\omega;\omega_0\delta_{iso},\omega_B). \qquad (8)$$

As shown in Fig. 3b-c, this exchange model successfully reproduced the ^{13}C spectra of pd@CO_2 and spd@CO_2 obtained

in 7.05 T with the Larmor frequency ω_0 of 75.3 MHz, with $k_B = 200$ Hz, $p_B = 0.628$ and $k_B = 200$ Hz, $p_B = 0.115$, respectively. To see the field dependence of the resonance lineshape, we measured ^{13}C NMR for the pd@CO_2 sample in another magnetic field of 14.09 T, and observed noticeable change in the pattern, as demonstrated in Fig. 3d. Since the chemical shift anisotropy is proportional to the field, the larger spectral distribution in the higher field prevents the resonance line from being averaged out by the exchange for a given set of the kinetic parameters. Thus, the shape of the resonance line obtained in the higher field (Fig. 3d) appeared to be closer to that with negligible exchange (Fig. 3a) than the resonance line obtained in the lower field (Fig. 3b) did. The spectrum could be fitted with that calculated based on our model, now with the Larmor frequency of 150.9 MHz, $k_B = 200$ Hz, and $p_B = 0.790$, which was somewhat different from that (0.628) for the data obtained in 7.05 T. The origin of such a discrepancy is unknown. Presumably, it stems from that there exists distribution in the size of the crystallites and thereby in the kinetic parameters, but the model assumes a single, well defined set of parameters. Forhcoming works need to address the effect of size distribution and experiments at different, various magnetic fields which were not available in the current studies.

^{13}C NMR spectra of sc@CO_2 and cc@CO_2 measured in 14.09 T did not show any discernible difference from those obtained in 7.05 T (Figs. S6 and S7). This is because that the exchange was already too slow in the lower field to affect the lineshape, and that the higher the magnetic field, the less the lineshape is affected by the exchange. Calculated lineshapes with other values of the parameters which did not fit the experimental ones are shown in Fig. S8.

The population p_B ranging from 0.6 to 0.8 obtained for pd@CO_2 indicates that the equilibrium is relatively biased toward the core site for the MDMOF crystallite with the sizes of the order of 10 μm. In contrast, the populations p_A and p_B of the isotropic and the core sites reversed for spd@CO_2, which means that the guest CO_2 molecules tend to be at the isotropic sites when the crystallites become as small as $\sim \mu$m.

A crude estimation of the thickness of the layer of the isotropic site can be made as follows. Let us consider cubic-shaped microcrystals with side lengths of 2 and 10 μm. When the thickness of the isotropic layer is assumed to be 0.5 μm, the ratio of the volume of isotropic site to the total volume are 0.875 and 0.271, respectively. These values are close to the population p_A of the isotropic sites of 0.885 for spd@CO_2 and of 0.29 for pd@CO_2 obtained from the fitting of the experimental ^{13}C resonance lines.

0.5 μm corresponds to ca. 500 unit cells in length. With this thickness of the isotropic layer, the side length longer than 100 μm would result in the ratio of the core volume to the isotropic one greater than 0.97, which can explain the reason why the ^{13}C spectra of sc@CO_2 and cc@CO_2 show the profile arising from the gyration of the CO_2 molecules alone.

To acquire the evidence for exchange across the crystallites, we carried out ^{13}C exchange spectroscopy (EXSY) experiments for $^{13}CO_2$ loaded in several, sub-millimeter-sized single crystals of NDMOF sealed together in a glass tube. As demonstrated in
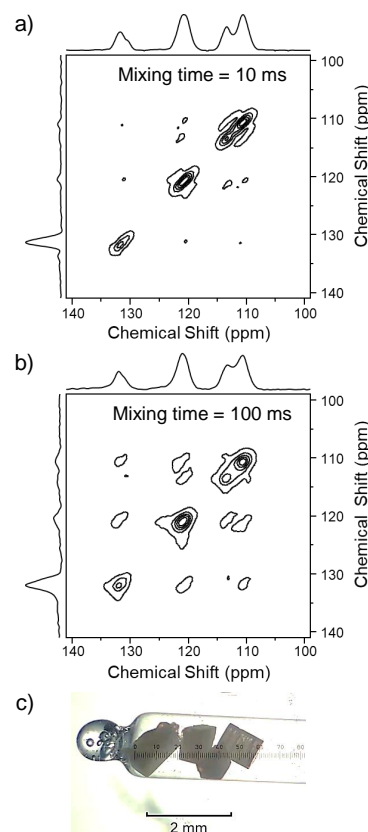
Fig. 5 ^{13}C EXSY spectra obtained in a $^{13}CO_2$ loaded glass tube containing several NDMOF single crystals with arbitrary orientations. The mixing time was 10 ms for (a) and 100 ms for (b). The EXSY experiments were performed at room temperature in a magnetic field of 7.05 T. (c) A photo of the NDMOF single crystals loaded glass tube for EXSY experiments.

Fig. 5, cross peaks were observed, and their intensity increased as the mixing time was prolonged from 10 ms to 100 ms. The growth of the cross peaks indicates that, for the NDMOF crystals with the size of the order of several hundreds of micrometers, the CO_2 molecules undergo exchange across the crystals in the time scale of the order of 100 ms, which, however, was rather long compared to the time scale (ca. 10 ms) of NMR signal acquisition.

In addition, the volume intensity of the cross peaks that reflects the portion of the CO_2 molecules participating such inter-crystal exchange was merely ca. 5 % of the intensity of the diagonal peaks. Thus, for the relatively large, sub-millimeter-sized NDMOF crystals, the lineshape of the one-dimensional ^{13}C NMR spectrum is expected to be unaffected by such slow and sparse exchange. This was also the case for cc@CO_2, since the spectrum in Fig. 3a could be explained by the gyration model alone. It is worth noting that previous works on CO_2 adsorption in different MOFs (DMOF-1, MOF-74) reported exchanges of the CO_2 molecules in a time scale of the order of hundreds of milliseconds[17,23], which is similar to that in the present work.

Even though the buildup behaviors of the cross peaks in the fine powder samples is of interest, the limited sensitivity did not allow us to acquire EXSY spectra of the pd@CO_2 and the spd@CO_2 samples within a practically feasible experimental time. Nevertheless, the mode and the rate of CO_2 exchange could be extracted from the shape of the resonance lines of the one-dimensional ^{13}C spectra shown in Fig. 3.

Since the kinetic parameters are also affected by temperature, the NMR spectrum is expected to change with temperature and be reproduced by the same model but with different values of the kinetic parameters and the populations. The translational motion at a different rate inside the host can cause the guest molecules to undergo reorientation in a different manner. Indeed, the temperature dependence observed for different type of MOFs was successfully explained by the the change in the apex angle of cone gyration[13,24].

4 Conclusions

The CO_2 molecules adsorbed in NDMOF undergo exchange among different crystallites and between the isotropic and the core sites. It is the size dependence of the rate of exchange that affects the size-dependent NMR lineshape. The particle-size effect that we observed in this work can also be seen in many other MOF-guest systems, and therefore needs attention in upcoming NMR investigations.

Author Contributions

Weiming Jiang: Conceptualization, Investigation, Visualization, Writing — original draft.
Kazuyuki Takeda: Supervision, Writing — review & editing.

Conflicts of interest

There are no conflicts to declare.

Acknowledgements

Notes and references

1 M. Ding, R. W. Flaig, H.-L. Jiang and O. M. Yaghi, *Chemical Society Reviews*, 2019, **48**, 2783–2828.

2 Q. Qian, P. A. Asinger, M. J. Lee, G. Han, K. Mizrahi Rodriguez, S. Lin, F. M. Benedetti, A. X. Wu, W. S. Chi and Z. P. Smith, *Chemical Reviews*, 2020, **120**, 8161–8266.

3 Q. Wang and D. Astruc, *Chemical Reviews*, 2020, **120**, 1438–1511.

4 M.-X. Wu and Y.-W. Yang, *Advanced Materials*, 2017, **29**, 1606134.

5 H.-Y. Li, S.-N. Zhao, S.-Q. Zang and J. Li, *Chemical Society Reviews*, 2020, **49**, 6364–6401.

6 F. Guo, S. Yang, Y. Liu, P. Wang, J. Huang and W.-Y. Sun, *ACS Catalysis*, 2019, **9**, 8464–8470.

7 K. Suresh, D. Aulakh, J. Purewal, D. J. Siegel, M. Veenstra and A. J. Matzger, *Journal of the American Chemical Society*, 2021, **143**, 10727–10734.

8 S. Krause, F. S. Reuter, S. Ehrling, V. Bon, I. Senkovska, S. Kaskel and E. Brunner, *Chemistry of Materials*, 2020, **32**, 4641–4650.

9 B. M. Connolly, M. Aragones-Anglada, J. Gandara-Loe, N. A. Danaf, D. C. Lamb, J. P. Mehta, D. Vulpe, S. Wuttke, J. Silvestre-Albero, P. Z. Moghadam, A. E. Wheatley and D. Fairen-Jimenez, *Nature Communications*, 2019, **10**, 1–11.

10 C. R. Marshall, J. P. Dvorak, L. P. Twight, L. Chen, K. Kadota, A. B. Andreeva, A. E. Overland, T. Ericson, A. F. Cozzolino and C. K. Brozek, *Journal of the American Chemical Society*, 2022, **144**, 5784–5794.

11 Y. Sakata, S. Furukawa, M. Kondo, K. Hirai, N. Horike, Y. Takashima, H. Uehara, N. Louvain, M. Meilikhov, T. Tsuruoka, S. Isoda, W. Kosaka, O. Sakata and S. Kitagawa, *Science*, 2013, **339**, 193–196.

12 O. M. Linder-Patton, W. M. Bloch, C. J. Coghlan, K. Sumida, S. Kitagawa, S. Furukawa, C. J. Doonan and C. J. Sumby, *CrystEngComm*, 2016, **18**, 4172–4179.

13 X. Kong, E. Scott, W. Ding, J. A. Mason, J. R. Long and J. A. Reimer, *Journal of the American Chemical Society*, 2012, **134**, 14341–14344.

14 L. C. Lin, J. Kim, X. Kong, E. Scott, T. M. McDonald, J. R. Long, J. A. Reimer and B. Smit, *Angewandte Chemie - International Edition*, 2013, **52**, 4410–4413.

15 M. Peksa, S. Burrekaew, R. Schmid, J. Lang and F. Stallmach, *Microporous and Mesoporous Materials*, 2015, **216**, 75–81.

16 M. Peksa, J. Lang and F. Stallmach, *Microporous and Mesoporous Materials*, 2015, **205**, 11–15.

17 A. C. Forse, M. I. Gonzalez, R. L. Siegelman, V. J. Witherspoon, S. Jawahery, R. Mercado, P. J. Milner, J. D. Martell, B. Smit, B. Blümich, J. R. Long and J. A. Reimer, *Journal of the American Chemical Society*, 2018, **140**, 1663–1673.

18 M. Sin, N. Kavoosi, M. Rauche, J. Pallmann, S. Paasch,

I. Senkovska, S. Kaskel and E. Brunner, *Langmuir*, 2019, **35**, 3162–3170.

19 P. Melix and T. Heine, *ChemPhysChem*, 2021, **22**, 2336–2341.

20 M. Mehring, *Principles of High Resolution NMR in Solids*, Springer-Verlag, Berlin, Heidelberg, New York, Second, re edn., 1983.

21 D. D. Do and K. Wang, *AIChE Journal*, 1998, **44**, 68–82.

22 V. Římal, H. Štěpánková and J. Štěpánek, *Concepts in Mag-*

netic Resonance Part A, 2011, **38A**, 117–127.

23 V. Bon, J. Pallmann, E. Eisbein, H. C. Hoffmann, I. Senkovska, I. Schwedler, A. Schneemann, S. Henke, D. Wallacher, R. A. Fischer, G. Seifert, E. Brunner and S. Kaskel, *Microporous and Mesoporous Materials*, 2015, **216**, 64–74.

24 R. M. Marti, J. D. Howe, C. R. Morelock, M. S. Conradi, K. S. Walton, D. S. Sholl and S. E. Hayes, *The Journal of Physical Chemistry C*, 2017, **121**, 25778–25787.